THE JOURNAL OF PHYSICAL CHEMISTRY Letters

Letter

Cite This: J. Phys. Chem. Lett. 2019, 10, 2386−2392

pubs.acs.org/JPCL

DNA-Templated Aggregates of Strongly Coupled Cyanine Dyes: Nonradiative Decay Governs Exciton Lifetimes

Jonathan S. Huff,[†] Paul H. Davis,[†] Allison Christy,[†] Donald L. Kellis,[†] Nirmala Kandadai,[‡] Zi S. D. Toa,[§] Gregory D. Scholes,[§] Bernard Yurke,*[,†,‡] William B. Knowlton,*[,†,‡] and Ryan D. Pensack*[,†]

[†]Micron School of Materials Science & Engineering and [‡]Department of Electrical & Computer Engineering, Boise State University, Boise, Idaho 83725, United States

[§]Department of Chemistry, Princeton University, Princeton, New Jersey 08544, United States

Supporting Information

ABSTRACT: Molecular excitons are used in a variety of applications including light harvesting, optoelectronics, and nanoscale computing. Controlled aggregation via covalent attachment of dyes to DNA templates is a promising aggregate assembly technique that enables the design of extended dye networks. However, there are few studies of exciton dynamics in DNA-templated dye aggregates. We report time-resolved excited-state dynamics measurements of two cyanine-based dye aggregates, a J-like dimer and an H-like tetramer, formed through DNA-templating of covalently attached dyes. Time-resolved fluorescence and transient absorption indicate that nonradiative decay, in the form of internal conversion, dominates the aggregate ground state recovery dynamics, with singlet exciton lifetimes on the order of tens of picoseconds for the aggregates versus nanoseconds for the monomer. These results highlight the importance of circumventing nonradiative decay pathways in the future design of DNA-templated dye aggregates.

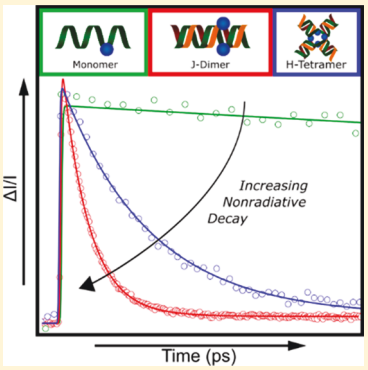

Excitons in molecular (dye) aggregates have sparked intense interest due to their potential applications in light harvesting (including natural,[1] artificial,[2,3] and biomimetic[4−6]), organic optoelectronics,[2,3] and more recently nanoscale computing.[7−11] Dye aggregation was first discovered in the 1930s when Jelley and Scheibe observed significant shifts in absorption spectra of concentrated cyanine dye solutions.[12−14] Since their discovery, considerable effort has been invested in developing an improved understanding of the structure of dye aggregates and nature of the attendant spectral shifts. Importantly, when interchromophore separations are similar to or less than the length of individual chromophores, where the term chromophore is defined as the light-absorbing portion of the dye molecule, electronic interactions result in splitting of the excited state energy levels and coherent delocalization of excitons. The magnitude of the energy level splitting (known as the Davydov splitting)[15] is highly sensitive to the interchromophore separation, while the relative orientation of the chromophore transition dipoles determines the selection rules for optical excitation of the molecular aggregates.

Figure 1 presents a summary schematic energy level diagram illustrating the excited state band splitting and selection rules for the simplest type of dye aggregates—dimers.[16,17] When chromophores are arranged such that their transition dipole moments align parallel to each other in an end to end fashion, the resulting chromophore assembly will display Jelley-aggregate (J-aggregate) behavior, with optical transitions allowed only to and from the lower energy excited state. Conversely, when the transition dipoles are instead stacked side-by-side in a parallel fashion, H-aggregate behavior is observed and optical transitions are only allowed to the higher energy excited state. For oblique configurations, wherein the transition dipole moments are not perfectly parallel, transitions to both excited state energy levels are allowed. From Figure 1, it is obvious that tuning the optical properties of aggregates requires fine spatial control over the dyes. Nature provides an example of such fine control in photosynthetic light harvesting complexes, which have evolved to maximize energy transfer efficiency.[18] While natural light harvesting systems use protein scaffolds to control intermolecular spacing and orientation, understanding protein folding and engineering artificial protein nanostructures is still in a nascent stage,[19−24] and hence rational design of artificial protein superstructures that incorporate and precisely template dyes is exceptionally difficult.

Using structurally less complex DNA oligonucleotides to assemble dye molecules has proven a more tractable approach to controlling aggregation.[4,6,25−29] The relatively simple rules of Watson−Crick base pairing enable the rational design of arbitrarily shaped DNA structures. This facile design process, combined with the wide range of commercially available dyes

Received: February 12, 2019
Accepted: April 23, 2019
Published: April 23, 2019

DOI: 10.1021/acs.jpclett.9b00404
J. Phys. Chem. Lett. 2019, 10, 2386−2392

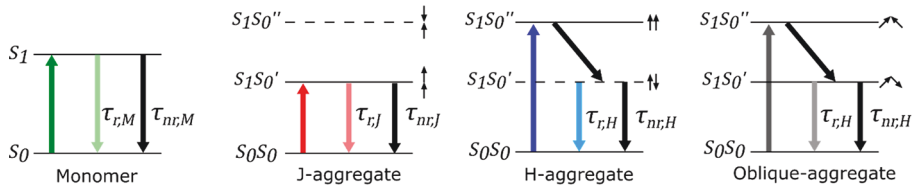

Figure 1. Schematic energy level diagrams of a dye monomer (far left), J-dimer (middle left), H-dimer (middle right), and oblique dimer (far right). A schematic representation of relative transition dipole moment orientations for each aggregate is shown to the right of each excitonic excited state. Solid horizontal lines indicate excitonic states that can couple optically to the ground state whereas dashed horizontal lines indicate excitonic states that cannot couple optically to the ground state. Optical transitions are shown as colored arrows for the monomer (green), J-aggregate (red), H-aggregate (blue), and oblique aggregate (gray). Optical (radiative) absorption is represented by dark colors, and optical (radiative) emission is represented by corresponding light colors. Nonradiative transitions are represented by black arrows.

and attendant labeling techniques for DNA, points toward the exciting prospect of using DNA to pattern coherently delocalized excitons. In particular, covalent attachment of dyes to the DNA backbone allows a high degree of spatial precision with regard to interchromophore spacing. Furthermore, the electronic coupling strength of DNA-templated dyes can be readily modulated by controlling the base pair (bp) separation.[4,6,25,28] A number of reports have demonstrated weak electronic coupling in the Förster regime achieved by spacing out dyes over large bp separations.[4,7−10,30−33] On the other hand, strong electronic coupling resulting in exciton delocalization (as evidenced by extensive spectral shifts and other optical phenomena), has only been reported in cases where dyes are positioned directly adjacent to one another on the same strand, or opposite each other on a DNA duplex and separated by no more than a single bp.[4,6,25,28,29,34−36]

Studies of the dynamics of molecular excitons in DNA-templated dye aggregates, which are critical to their application in excitonic devices, are unfortunately scarce. In particular, the excited-state lifetime, which can change upon aggregation, is a parameter of crucial importance. Long exciton lifetimes enhance exciton transmission distance and enable more complex structures. Conversely, short lifetimes may limit the use of excitons for optoelectronic and nanoscale computing applications, highlighting the need to optimize lifetimes. While existing time-resolved studies of strongly coupled DNA-templated dye aggregates report reduced exciton lifetimes relative to the respective monomers,[6,37,38] the mechanisms suggested for the reduced exciton lifetimes differ. One recent work suggests that aggregation enhances photoisomerization in covalently templated Cy3 dimers, thereby increasing the nonradiative decay rate and reducing the excited-state lifetime.[6] In contrast, recent work with DNA-intercalated pseudoisocyanine J-aggregates has suggested that the observed accelerated exciton dynamics result from superradiant emission enhancement.[37,38] However, it is unclear whether both processes are active in these systems, and if so, to what degree.

In this Letter, we report the excited-state relaxation dynamics of two DNA-templated Cy5 dye systems that exhibit spectral signatures characteristic of strong excitonic coupling. Two representative systems were selected for this study, with one system exhibiting primarily J-aggregate behavior (i.e., J-*like* behavior) and the other primarily H-aggregate behavior (i.e., H-*like* behavior). Initial measurements utilizing steady-state spectroscopic techniques resulted in two key observations. First, a subpopulation of highly fluorescent monomers remains in solution despite purification of the as-formed constructs. This subpopulation of monomers is accounted for in all subsequent measurements. Second, solutions of both J-like and H-like aggregate systems exhibit low fluorescence quantum yields relative to the monomer, suggesting enhanced nonradiative pathways. Subsequently, time-resolved fluorescence (TRF) and transient absorption spectroscopy (TAS) measurements are presented, showing that exciton lifetimes for both the H-like and J-like aggregates are nearly 2 orders of magnitude shorter than that of the monomer. A quantitative analysis of the exciton lifetimes and fluorescence quantum yields indicates that nonradiative decay, in contrast to superradiance, governs exciton lifetimes in both these aggregate systems.

Following the work of Cannon et al.,[25] two DNA-templated Cy5 aggregate constructs were selected for this work: (i) a hybridized DNA duplex bearing a pair of Cy5 dyes located directly across from each other on opposing strands (i.e., 0 bp separation) that form a strongly coupled J-like dimer (Figure 2, middle) and (ii) a four-armed mobile Holliday junction that results in a strongly coupled H-like tetramer of Cy5 molecules at 0 bp separation (Figure 2, bottom). In both constructs, each dye molecule is covalently attached at either end to the DNA backbone via a pair of linkers. Cy5 was chosen because, in

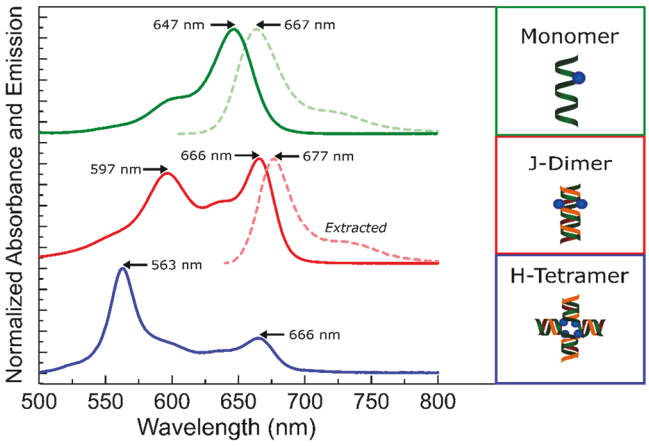

Figure 2. Steady-state absorption and fluorescence emission spectra with corresponding schematic illustrations for the DNA-templated Cy5 monomer (top), J-dimer (middle), and H-tetramer (bottom). The absorption spectra for the monomer, J-dimer, and H-tetramer are plotted in dark green, red, and blue, respectively, and the emission spectra for the monomer and J-dimer are plotted as dashed lines in light green and light red, respectively. The emission spectra for both the monomer and J-dimer were obtained using an excitation wavelength of 595 nm, with the fluorescence emission of the J-dimer extracted via the method described in the Supporting Information, section S.6. As described in the main text, it was not possible to extract the H-tetramer emission spectrum.

DOI: 10.1021/acs.jpclett.9b00404
J. Phys. Chem. Lett. 2019, 10, 2386−2392

addition to being readily attached to DNA, its high molar extinction coefficient (>200 000 M^{-1} cm^{-1}) lends itself to strong excitonic coupling and its high fluorescence quantum yield indicates few intrinsic nonradiative decay pathways. Constructs were prepared in aqueous buffer solution according to Cannon et al.[25] To ensure the removal of malformed structures and excess monomer strands, the aggregate solutions were purified by polyacrylamide gel electrophoresis (PAGE, see Supporting Information, section S.1). For steady-state absorption and fluorescence measurements, samples were prepared with an optical density of 0.1 or less at the highest absorption peak; for time-resolved fluorescence and transient absorption measurements, the optical densities at the highest absorption peak were less than 0.1 and 0.3, respectively. Additional details regarding optical spectroscopy measurements and associated sample preparation can be found in Supporting Information, section S.2.

The constructs were characterized via steady-state absorption spectroscopy, which provides information regarding the type and extent of electronic coupling induced by aggregation. The absorption spectrum of a single-stranded Cy5-labeled oligonucleotide, which forms the basis for both aggregate constructs, is displayed in Figure 2 (top). This Cy5 monomer spectrum exhibits a single electronic absorption band, with the vibronic origin (i.e., 0−0) band peaking at ca. 647 nm. The J-dimer (Figure 2, middle) exhibits both a blue-shifted peak at ca. 597 nm and a more intense red-shifted peak at ca. 666 nm, while the H-tetramer (Figure 2, bottom) exhibits a very intense blue-shifted peak (ca. 563 nm) and suppressed absorption intensity at longer wavelengths, both signatures of strong electronic coupling in the aggregate samples (Figure 1). With the exception of the J-dimer solution's absorption spectrum, which exhibits signatures of a small amount of structural heterogeneity due to slight variations in sample preparation (see Supporting Information, section S.3), these results are consistent with Cannon et al.,[25] who also provided the dye packing geometries associated with each of these constructs as determined via a detailed theoretical analysis of the absorption spectra.

Steady-state fluorescence spectroscopy provides additional, complementary information about the electronic structure of the samples. The Cy5 monomer fluorescence emission is readily measured given its appreciable fluorescence quantum yield (Φ_F = 0.29, see Supporting Information, section S.4), and the resultant emission spectrum is essentially a mirror image of the absorption spectrum (Figure 2, top). On the basis of the difference in energy between the absorption and fluorescence origin bands (with the latter peaking at 667 nm), the Stokes shift for the monomer was found to be ca. 440 cm^{-1}. These values are generally consistent with prior literature reports.[29] Initial attempts to measure the fluorescence emission of the J- and H-aggregate samples were thwarted by their highly suppressed emission intensity as compared to the monomer (fluorescence quantum yields for the J- and H-aggregate solutions were ca. 1×10^{-2} and 3×10^{-4}, respectively). Upon further inspection, fluorescence excitation measurements indicated that an additional, extremely low concentration monomer component (i.e., a subpopulation of structures that exhibited optical signatures of monomers) contributed non-negligibly to the observed fluorescence emission of both PAGE-purified aggregate solutions (Supporting Information, section S.5). Accordingly, a procedure was developed to extract the "pure" emission spectrum of each aggregate component from the corresponding as-measured fluorescence data (Supporting Information, section S.6). The resultant extracted J-dimer emission spectrum is displayed in Figure 2, middle. The origin band of the J-dimer emission peaks at ca. 677 nm, which is slightly red-shifted with respect to the origin band of the J-dimer absorption (ca. 666 nm). The corresponding Stokes shift of ca. 240 cm^{-1} for the J-dimer is much smaller than the 440 cm^{-1} Stokes shift measured for the monomer, consistent with J-aggregation.[39] Due to the even more highly suppressed fluorescence emission of the H-tetramer construct, it was not possible to extract the H-tetramer's "pure" emission spectrum in the same manner as the J-dimer, although a broad, featureless, red-shifted emission band was observed at ca. 800 nm (Supporting Information, section S.7). Similar broad, featureless fluorescence emission, reminiscent of that seen from molecular "excimers",[40] has been observed previously for H-aggregates of other cyanine-based dyes.[41,42] Critically, the fluorescence quenching observed in the aggregate solutions suggests the presence of a significant nonradiative decay pathway in the aggregates that is not present in the monomer.

With the steady-state behavior of the aggregate constructs characterized, the exciton dynamics were investigated using a time-resolved fluorescence method, time-correlated single photon counting (TCSPC). On the basis of each construct's respective absorption spectrum (Figure 2) and available excitation wavelengths, an excitation wavelength of 653 nm was selected for the monomer and J-dimer samples, while 507 nm was chosen to excite the H-tetramer sample. The fluorescence was then monitored near the maximum emission wavelength for each sample, corresponding to detection wavelengths of 667, 680, and 800 nm for the monomer, J-dimer, and H-tetramer samples, respectively. The detection wavelengths of 680 and 800 nm for the J-dimer and H-tetramer, respectively, were chosen to maximize the aggregate contribution and minimize the monomer contribution to the overall fluorescence decay. The resultant fluorescence decays are shown as open circles in Figure 3, with corresponding exponential decay fits shown as lines. The fluorescence decay of the monomer (Figure 3, green) was well described by a single exponential with a time constant of τ = 1.3 ns, in excellent agreement with previously reported excited-state lifetimes for Cy5.[4,43,44] Interestingly, the J-dimer and H-tetramer both exhibited much faster decays than the monomer. Because of the additional subpopulation of monomers present in these samples, a biexponential function was necessary to properly fit the data (Supporting Information, section S.8). The TCSPC data for the J-dimer and H-tetramer samples fit in this manner yielded a long time component of ca. 1.3 ns, consistent with a monomer contribution to the fluorescence, and a second short, instrument response limited decay component with a time constant less than ca. 250 ps. The fit parameters obtained are displayed in Table 1. The larger monomer subpopulation component contribution (A_2 in Table 1) in the J-dimer experiment is due to the fact that the monomer and J-dimer exhibit similar optical properties (i.e., absorption and emission spectra, Figure 2) and so there is poor contrast between these components at the excitation and emission wavelengths, whereas the H-tetramer absorption and emission are well separated from that of the monomer.

Insight into the nature of the accelerated fluorescence decay of the aggregates, i.e., whether radiative or nonradiative relaxation plays a dominant role, can be gleaned by considering the TCSPC results in the context of molecular exciton theory.

DOI: 10.1021/acs.jpclett.9b00404
J. Phys. Chem. Lett. 2019, 10, 2386−2392

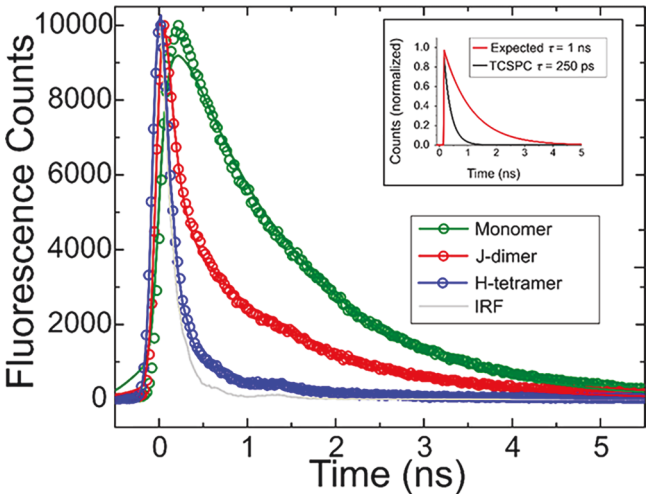

Figure 3. Time-resolved fluorescence decays of solutions of the monomer (green), J-dimer (red), and H-tetramer (blue). The instrument response function (IRF) is shown in solid gray. Open circles correspond to the experimental data, while the solid lines represent exponential decay fits convolved with the IRF. Inset: The observed (black trace) versus expected (red trace) fluorescence decays for the J-dimer. The expected decay assumes classical (Kasha-type) J-aggregate behavior, and that aggregation only affects the radiative decay rate (i.e., it assumes that $k_{nr,J} = k_{nr,m}$). For the purpose of illustrating the limiting case of full superradiance, it also assumes the maximum radiative rate possible, which for a dimer is $k_{r,J} = 2 \times k_{r,m}$. Full details of the derivation are reported in Supporting Information, section S.9.

Table 1. Excitation Wavelengths and Biexponential Fitting Parameters for TCSPC Decays[a]

construct	λ_{exc} (nm)	A_1 (%)	τ_1 (ns)	A_2 (%)	τ_2 (ns)
monomer	653	N/A	1.3	N/A	N/A
J-dimer	653	87	≤0.25	13	1.3
H-tetramer	507	99.8	≤0.25	0.2	1.3

[a]The decays corresponding to the aggregate constructs were fit with the following biexponential function: $I(t) = A_1 e^{-t/\tau_1} + A_2 e^{-t/\tau_2}$. See Supporting Information, section S.8 for additional details regarding the mathematical and physical justification of these biexponential fits.

First, it is instructive to consider that the observed decay rate, k_{obs}, is equal to the sum of the radiative, k_r, and nonradiative, k_{nr}, decay rates (i.e., $k_{obs} = k_r + k_{nr}$).[45] The first of these terms, k_r, can be evaluated according to molecular exciton theory.[17,46] For example, k_r is enhanced in a J-aggregate, an effect known colloquially as superradiance.[47] In an ideal J-aggregate (Figure 1, middle left), $k_{r,J}$ is equivalent to the product of the number of molecules comprising the aggregate, N, and the radiative rate of a single molecule (i.e., $k_{r,J} = N \times k_{r,m}$).[47,48] Conversely, for an H-aggregate, $k_{r,H}$ is suppressed and, for an ideal H-aggregate (Figure 1, middle right) where the optical transition between the lowest excited state (S_1S_0') and the ground state (S_0S_0) is forbidden, $k_{r,H} = 0$. Because molecules typically pack in an oblique manner (Figure 1, right) or in a manner that is neither pure J nor H, these ideal limits generally are not realized. More typically, mixed J- or H-like behavior is observed, as in the present case (Figure 2). For these real systems, insights into the radiative decay rate can be gleaned from the experimentally measured extinction spectrum. For example, Strickler and Berg showed that the radiative rate is directly related to the intensity of absorption into the lowest-energy singlet excited state.[49] While a quantitative analysis of the radiative decay rate of the J- and H-like constructs is complicated by several factors, including structural heterogeneity and overlapping transitions to $(S_1S_0)'$ and $(S_1S_0)''$ states, we know from prior work[25] that the extinction of their lowest-energy singlet absorption band is increased and decreased, respectively. Relative to the monomer ($k_{r,m}$), we can therefore expect the radiative rate to be enhanced for the J-dimer ($k_{r,J}$) and suppressed for the H-tetramer ($k_{r,H}$), where m, J, and H, indicate the monomer, J-dimer, and H-tetramer, respectively.

Considering that exciton theory predicts an enhanced and suppressed k_r for the J-dimer and H-tetramer, respectively, and employing the previous assumption that k_{nr} is uninfluenced by aggregation (i.e., $k_{nr,aggregate} = k_{nr,m}$), we expect k_{obs} for the J-dimer and H-tetramer to be enhanced and suppressed, respectively. Figure 3 shows that the fluorescence decay of the H-tetramer is significantly accelerated with respect to the monomer. Since an aggregation-induced decrease in k_r should serve to *increase* the fluorescence lifetime of the H-tetramer, this unexpected observed decrease in the fluorescence lifetime can only be accounted for by a significant increase in the nonradiative rate for the H-tetramer, $k_{nr,H}$. Figure 3 shows that the fluorescence decay of the J-dimer is also significantly accelerated with respect to the monomer. Here, we can place bounds on the extent to which superradiance contributes to the overall enhanced decay. By covalently tethering two Cy5 dyes to the DNA template, we can guarantee that two, and only two, dye molecules interact. This means that we can expect a $k_{r,J}$ rate enhancement of at most $2 \times k_{r,m}$. The inset of Figure 3 shows the fluorescence decay expected for the J-dimer according to these assumptions, which yields a time constant of 1.0 ns (red curve; see Supporting Information, section S.9). Also shown in the Figure 3 inset is a single exponential decay generated for the J-dimer based on the measured, instrument response-limited fluorescence lifetime (black curve), which decays considerably faster than the decay expected for solely radiative enhancement (red trace). This discrepancy between the expected and actual fluorescence decay rates shows that new and significant nonradiative decay channels emerge in the J-dimer. Hence, for both types of aggregates, the TCSPC measurements confirm that significantly enhanced nonradiative relaxation is introduced upon aggregation.

In order to better understand the nonradiative relaxation in the aggregate constructs, we turned to ultrafast transient absorption spectroscopy (TAS). Significantly, TAS provides information on both bright and dark states, such as triplets and photoisomers, and can additionally elucidate whether the initial photoexcitation returns directly to the ground state and, if so, on what time scale. Furthermore, since the response time of the TAS system is nearly 3 orders of magnitude faster than the TCSPC system (Supporting Information, section S.10), we can potentially directly time resolve the excited state decay and quantify the extent of the nonradiative relaxation contribution. For the TAS measurements, each sample was excited and probed near its respective absorption maximum for maximal signal-to-noise, with wavelengths of 650, 675, and 565 nm used for the monomer, J-dimer, and H-tetramer, respectively (Supporting Information, section S.11). Note that to improve contrast with the underlying subpopulation of monomers, the J-dimer sample was excited and probed at 675 nm, which is slightly red-shifted relative to its absorption maximum (see Figure 2).

DOI: 10.1021/acs.jpclett.9b00404
J. Phys. Chem. Lett. 2019, 10, 2386−2392

The transient absorption (TA) decays for the monomer and aggregate samples are displayed in Figure 4. All samples show a

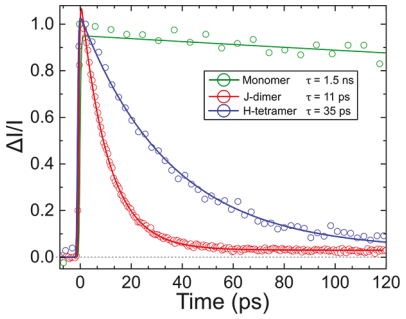

Figure 4. Transient absorption measurements on solutions of the monomer (green), J-dimer (red), and H-tetramer (blue). The open circles correspond to the experimental data, while the solid lines represent single or biexponential fits to the data (see main text for additional details). The data are scaled to unity with a positive scalar to preserve the sign of the signal.

positive ground state bleach signal that decays with time. A single exponential fit described the monomer TA decay well and returned a time constant of 1.5 ns, in good agreement with the lifetime measured by TCSPC. Furthermore, the recovery of the ground-state bleach signal to baseline indicates that the monomer relaxes directly to the ground state with very low probability of photoisomerization or intersystem crossing.[50] For the aggregate solutions, a significantly more rapid initial recovery of the ground state bleach is observed. As with the TCSPC data, an additional long-time component consistent with a subpopulation of monomers was observed, and hence a biexponential fit was necessary to accurately model these data. Significantly, the short time constants corresponding to ground state recovery of the aggregate species were found to be 11 and 35 ps for the J-dimer and H-tetramer, respectively. Wavelength- and fluence-dependence measurements (Supporting Information, sections S.12 and S.13) indicate that the measured lifetimes are representative of the intrinsic exciton lifetimes; that is, the measurements are not complicated by additional decay pathways, such as internal conversion from high-lying excited states or exciton−exciton annihilation, nor the structural heterogeneity identified in Supporting Information, section S.3. Quantitative analysis of the TA data (Supporting Information, section S.14) reveals the excited-state dynamics of the aggregate constructs are nearly exclusively governed by nonradiative processes, with 99.6% of ground state recovery being nonradiative in nature for the J-dimer and 99.96% nonradiative for the H-tetramer.

Having quantified the nonradiative contribution to the overall decay, the underlying microscopic decay mechanism can be examined. In view of the rapid nature of the nonradiative relaxation of the aggregate constructs (i.e., tens of picoseconds), both intersystem crossing and photoisomerization can be ruled out as contributing significantly to the nonradiative decay. While intersystem crossing and photoisomerization can be rapid in certain systems, these processes occur on a microsecond time scale for Cy5 attached to DNA,[50] and it is difficult to envision how aggregation would accelerate their kinetics by nearly 6 orders of magnitude. For example, there are no "heavy atoms" in this Cy5 derivative (Supporting Information, section S.1) to facilitate intersystem crossing in the aggregate constructs, and steric hindrance due to the presence of adjacent molecules would tend to decrease rather than increase the rate of photoisomerization. Additionally, charge transfer is ruled out for reasons discussed in the Supporting Information, section S.15. A seminal contribution by Sundström and Gillbro studying dithiadicarbocyanine, a compound structurally very similar to Cy5, also observed drastically accelerated nonradiative decay in aggregated systems.[51] In that work, the authors concluded the nonradiative decay was facilitated by an electric dipole−dipole coupling mechanism; this, however, was later disputed[52] on the basis that the trend the authors observed for the exciton lifetime with respect to the dielectric constant of the medium was inconsistent with a decay mechanism based on electric dipole−dipole coupling. These previous studies[50,52] indicate that, in addition to nonradiative decay via photoisomerization and intersystem crossing, nonradiative decay via electric dipole−dipole coupling can be ruled out. This indicates direct relaxation to the ground state via strong nonadiabatic coupling, i.e., internal conversion, must be the dominant mechanism governing the short exciton lifetimes of the Cy5 aggregates. Given that such rapid nonradiative relaxation is observed in both H- and J-aggregates of even more structurally rigid compounds (e.g., cresyl violet,[53,54] methylene blue,[51,52] and structurally very similar thionine,[51,55] Nile blue,[56] porphyrins,[57−59] and phthalocyanines[60,61]) where photoinduced isomerization is not possible, we further conclude that radiationless, nonadiabatic transitions from S_1S_0 directly to S_0S_0 (and, in the present case, the thermally stable *trans* isomer[62] form of S_0S_0) may represent a general decay pathway that emerges in systems comprising excitonically coupled dye aggregates.

In conclusion, we have investigated the excited-state dynamics of strongly coupled J-aggregate (dimer) and H-aggregate (tetramer) constructs formed through covalent attachment of cyanine-based (Cy5) dyes to DNA. Steady-state absorption and fluorescence spectroscopy indicated that fluorescence emission was strongly quenched in the aggregate solutions, and the majority of this emission arises from a small subpopulation of highly emissive monomers. Quenched fluorescence emission suggests that a new nonradiative decay pathway is introduced upon aggregation, which was confirmed via an analysis of TCSPC measurements in the context of molecular exciton theory. Finally, the extent to which nonradiative decay contributes to the relaxation dynamics was quantified with TAS. The exciton lifetimes of the J-dimer and H-tetramer were measured to be ca. 11 and 35 ps, respectively, indicating that nonradiative decay is largely (>99%) responsible for the relaxation dynamics of both types of aggregates studied here, which we attribute to a rapid nonadiabatic transition between S_1S_0 and S_0S_0. Identifying the dominant relaxation mechanism in DNA-templated dye aggregates as direct internal conversion to the ground state presents the tantalizing possibility of optimally tuning exciton lifetimes for optoelectronic and nanoscale computing applications by rationally modifying either the DNA backbone or dye structure.

■ ASSOCIATED CONTENT

Supporting Information

The Supporting Information is available free of charge on the ACS Publications website at DOI: 10.1021/acs.jpclett.9b00404.

DOI: 10.1021/acs.jpclett.9b00404
J. Phys. Chem. Lett. 2019, 10, 2386−2392

Section S.1, dye structure, DNA sequences, construct preparation, and purification procedure; section S.2, optical spectroscopy experimental methods; section S.3, origin of absorption spectrum variation—evidence for structural heterogeneity in J-dimer solution; section S.4, Monomer Photophysics ; section S.5: Fluorescence Excitation Spectroscopy Establishes the Multicomponent Nature of Aggregate Solutions; section S.6: extraction of the "pure" J-dimer emission spectrum; section S.7, H-tetramer solution emission; section S.8, mathematical and physical justification of biexponential fits for aggregate solution time-resolved fluorescence; section S.9, derivation of expected fluorescence decay rate for J-aggregates; section S.10, transient absorption pulse characterization; section S.11, comparison of sample absorption spectra and laser spectra; section S.12, ground state recovery of aggregates independent of excitation wavelength; section S.13, ground state recovery of aggregates independent of incident pump fluence; section S.14, quantitative analysis of radiative and nonradiative rates; and section S.15, charge transfer ruled out as a nonradiative decay mechanism (PDF)

AUTHOR INFORMATION

Corresponding Authors

*(W.B.K.) bknowlton@boisestate.edu.
*(B.Y.) bernardyurke@boisestate.edu.
*(R.D.P.) ryanpensack@boisestate.edu.

ORCID

Jonathan S. Huff: 0000-0002-2025-9605
Paul H. Davis: 0000-0001-7333-8748
Donald L. Kellis: 0000-0002-1837-492X
Zi S. D. Toa: 0000-0003-2890-6579
Gregory D. Scholes: 0000-0003-3336-7960
Bernard Yurke: 0000-0003-3913-2855
William B. Knowlton: 0000-0003-3018-2207
Ryan D. Pensack: 0000-0002-1302-1770

Notes

The authors declare no competing financial interest.

ACKNOWLEDGMENTS

Work at Boise State University was supported by the National Science Foundation (NSF), INSPIRE No. 1648655 and NSF MRI Award 0923541. Portions of this work were also supported by the Department of Energy (DOE), LDRD No. 154754. Z.S.D.T. and G.D.S. acknowledge support from the Division of Chemical Sciences, Geosciences, and Biosciences, Office of Basic Energy Sciences of the U.S. DOE, through Grant No. DE-SC0019370. The authors would like to thank J. Mellinger, P. Cunningham, and J. Dean for useful comments on the manuscript and B. Cannon, whose preliminary results guided the temperature-dependent UV−vis measurements reported in the Supporting Information.

REFERENCES

(1) Mirkovic, T.; Ostroumov, E. E.; Anna, J. M.; van Grondelle, R.; Govindjee; Scholes, G. D. Light Absorption and Energy Transfer in the Antenna Complexes of Photosynthetic Organisms. *Chem. Rev.* **2017**, *117* (2), 249−293.

(2) Ostroverkhova, O. Organic Optoelectronic Materials: Mechanisms and Applications. *Chem. Rev.* **2016**, *116* (22), 13279−13412.

(3) Brixner, T.; Hildner, R.; Köhler, J.; Lambert, C.; Würthner, F. Exciton Transport in Molecular Aggregates − From Natural Antennas to Synthetic Chromophore Systems. *Adv. Energy Mater.* **2017**, *7* (16), 1700236.

(4) Cunningham, P. D.; Khachatrian, A.; Buckhout-White, S.; Deschamps, J. R.; Goldman, E. R.; Medintz, I. L.; Melinger, J. S. Resonance Energy Transfer in DNA Duplexes Labeled with Localized Dyes. *J. Phys. Chem. B* **2014**, *118* (50), 14555−14565.

(5) Melinger, J. S.; Khachatrian, A.; Ancona, M. G.; Buckhout-White, S.; Goldman, E. R.; Spillmann, C. M.; Medintz, I. L.; Cunningham, P. D. FRET from Multiple Pathways in Fluorophore-Labeled DNA. *ACS Photonics* **2016**, *3* (4), 659−669.

(6) Cunningham, P. D.; Kim, Y. C.; Díaz, S. A.; Buckhout-White, S.; Mathur, D.; Medintz, I. L.; Melinger, J. S. Optical Properties of Vibronically Coupled Cy3 Dimers on DNA Scaffolds. *J. Phys. Chem. B* **2018**, *122* (19), 5020−5029.

(7) Graugnard, E.; Kellis, D. L.; Bui, H.; Barnes, S.; Kuang, W.; Lee, J.; Hughes, W. L.; Knowlton, W. B.; Yurke, B. DNA-Controlled Excitonic Switches. *Nano Lett.* **2012**, *12* (4), 2117−2122.

(8) Cannon, B. L.; Kellis, D. L.; Davis, P. H.; Lee, J.; Kuang, W.; Hughes, W. L.; Graugnard, E.; Yurke, B.; Knowlton, W. B. Excitonic AND Logic Gates on DNA Brick Nanobreadboards. *ACS Photonics* **2015**, *2* (3), 398−404.

(9) Kellis, D. L.; Rehn, S. M.; Cannon, B. L.; Davis, P. H.; Graugnard, E.; Lee, J.; Yurke, B.; Knowlton, W. B. DNA-Mediated Excitonic Upconversion FRET Switching. *New J. Phys.* **2015**, *17* (11), 115007.

(10) Wang, S.; Lebeck, A. R.; Dwyer, C. Nanoscale Resonance Energy Transfer-Based Devices for Probabilistic Computing. *IEEE Micro* **2015**, *35* (5), 72−84.

(11) Sawaya, N. P. D.; Rappoport, D.; Tabor, D. P.; Aspuru-Guzik, A. Excitonics: A Set of Gates for Molecular Exciton Processing and Signaling. *ACS Nano* **2018**, *12* (7), 6410−6420.

(12) Jelley, E. E. Spectral Absorption and Fluorescence of Dyes in the Molecular State. *Nature* **1936**, *138* (3502), 1009−1010.

(13) Jelley, E. E. Molecular, Nematic and Crystal States of I: I-Diethyl–Cyanine Chloride. *Nature* **1937**, *139* (3519), 631.

(14) Scheibe, G. Über Die Veränderlichkeit Der Absorptionsspektren in Lösungen Und Die Nebenvalenzen Als Ihre Ursache. *Angew. Chem.* **1937**, *50* (11), 212−219.

(15) Davydov, A. S. Theory of Absorption Spectra of Molecular Crystals. *Transl. Repr. from Zh. Eksp. Teor. Fiz.* **1948**, *18* (2), 210−218.

(16) Kasha, M. Energy Transfer Mechanisms and the Molecular Exciton Model for Molecular Aggregates. *Radiat. Res.* **1963**, *20* (1), 55−70.

(17) Kasha, M.; Rawls, H. R.; Ashraf El-Bayoumi, M. The Exciton Model in Molecular Spectroscopy. *Pure Appl. Chem.* **1965**, *11* (3−4), 371−392.

(18) Scholes, G. D.; Fleming, G. R.; Olaya-Castro, A.; Van Grondelle, R. Lessons from Nature about Solar Light Harvesting. *Nat. Chem.* **2011**, *3* (10), 763−774.

(19) Snow, C. D.; Nguyen, H.; Pande, V. S.; Gruebele, M. Absolute Comparison of Simulated and Experimental Protein-Folding Dynamics. *Nature* **2002**, *420* (6911), 102−106.

(20) Baker, D.; Sali, A. Protein Structure Prediction and Structural Genomics. *Science* **2001**, *294* (5540), 93−96.

(21) Dill, K. A.; MacCallum, J. L. The Protein-Folding Problem, 50 Years On. *Science* **2012**, *338* (6110), 1042−1046.

(22) Yeates, T. O. Geometric Principles for Designing Highly Symmetric Self-Assembling Protein Nanomaterials. *Annu. Rev. Biophys.* **2017**, *46* (1), 23−42.

(23) Huang, P. S.; Boyken, S. E.; Baker, D. The Coming of Age of de Novo Protein Design. *Nature* **2016**, *537* (7620), 320−327.

(24) Bale, J. B.; Gonen, S.; Liu, Y.; Sheffler, W.; Ellis, D.; Thomas, C.; Cascio, D.; Yeates, T. O.; Gonen, T.; King, N. P.; et al. Accurate Design of Megadalton-Scale Two-Component Icosahedral Protein Complexes. *Science* **2016**, *353* (6297), 389−395.

DOI: 10.1021/acs.jpclett.9b00404
J. Phys. Chem. Lett. 2019, 10, 2386−2392

(25) Cannon, B. L.; Kellis, D. L.; Patten, L. K.; Davis, P. H.; Lee, J.; Graugnard, E.; Yurke, B.; Knowlton, W. B. Coherent Exciton Delocalization in a Two-State DNA-Templated Dye Aggregate System. *J. Phys. Chem. A* **2017**, *121* (37), 6905−6916.
(26) Cannon, B. L.; Patten, L. K.; Kellis, D. L.; Davis, P. H.; Lee, J.; Graugnard, E.; Yurke, B.; Knowlton, W. B. Large Davydov Splitting and Strong Fluorescence Suppression: An Investigation of Exciton Delocalization in DNA-Templated Holliday Junction Dye Aggregates. *J. Phys. Chem. A* **2018**, *122* (8), 2086−2095.
(27) Teo, Y. N.; Kool, E. T. DNA-Multichromophore Systems. *Chem. Rev.* **2012**, *112* (7), 4221−4245.
(28) Nicoli, F.; Roos, M. K.; Hemmig, E. A.; Di Antonio, M.; De Vivie-Riedle, R.; Liedl, T. Proximity-Induced H-Aggregation of Cyanine Dyes on DNA-Duplexes. *J. Phys. Chem. A* **2016**, *120* (50), 9941−9947.
(29) Markova, L. I.; Malinovskii, V. L.; Patsenker, L. D.; Häner, R. J-vs. H-Type Assembly: Pentamethine Cyanine (Cy5) as a near-IR Chiroptical Reporter. *Chem. Commun.* **2013**, *49* (46), 5298−5300.
(30) Melinger, J. S.; Khachatrian, A.; Ancona, M. G.; Buckhout-White, S.; Goldman, E. R.; Spillmann, C. M.; Medintz, I. L.; Cunningham, P. D. FRET from Multiple Pathways in Fluorophore-Labeled DNA. *ACS Photonics* **2016**, *3* (4), 659−669.
(31) Klein, W. P.; Díaz, S. A.; Buckhout-White, S.; Melinger, J. S.; Cunningham, P. D.; Goldman, E. R.; Ancona, M. G.; Kuang, W.; Medintz, I. L. Utilizing HomoFRET to Extend DNA-Scaffolded Photonic Networks and Increase Light-Harvesting Capability. *Adv. Opt. Mater.* **2018**, *6* (1), 1870005.
(32) Heilemann, M.; Tinnefeld, P.; Sanchez Mosteiro, G.; Garcia Parajo, M.; Van Hulst, N. F.; Sauer, M. Multistep Energy Transfer in Single Molecular Photonic Wires. *J. Am. Chem. Soc.* **2004**, *126* (21), 6514−6515.
(33) Massey, M.; Medintz, I. L.; Ancona, M. G.; Algar, W. R. Time-Gated FRET and DNA-Based Photonic Molecular Logic Gates: AND, OR, NAND, and NOR. *ACS Sensors* **2017**, *2* (8), 1205−1214.
(34) Asanuma, H.; Fujii, T.; Kato, T.; Kashida, H. Coherent Interactions of Dyes Assembled on DNA. *J. Photochem. Photobiol., C* **2012**, *13* (2), 124−135.
(35) Kringle, L.; Sawaya, N. P. D.; Widom, J.; Adams, C.; Raymer, M. G.; Aspuru-Guzik, A.; Marcus, A. H. Temperature-Dependent Conformations of Exciton-Coupled Cy3 Dimers in Double-Stranded DNA. *J. Chem. Phys.* **2018**, *148* (8), 085101.
(36) Heussman, D.; Kittell, J.; Kringle, L.; Tamimi, A.; von Hippel, P. H.; Marcus, A. H. Measuring Local Conformations and Conformational Disorder of (Cy3)2 Dimer Labeled DNA Fork Junctions Using Absorbance, Circular Dichroism and Two-Dimensional Fluorescence Spectroscopy. *Faraday Discuss.* **2019**, DOI: 10.1039/C8FD00245B.
(37) Banal, J. L.; Kondo, T.; Veneziano, R.; Bathe, M.; Schlau-Cohen, G. S. Photophysics of J-Aggregate-Mediated Energy Transfer on DNA. *J. Phys. Chem. Lett.* **2017**, *8* (23), 5827−5833.
(38) Boulais, E.; Sawaya, N. P. D.; Veneziano, R.; Andreoni, A.; Banal, J. L.; Kondo, T.; Mandal, S.; Lin, S.; Schlau-Cohen, G. S.; Woodbury, N. W.; et al. Programmed Coherent Coupling in a Synthetic DNA-Based Excitonic Circuit. *Nat. Mater.* **2018**, *17* (2), 159−166.
(39) Würthner, F.; Kaiser, T. E.; Saha-Möller, C. R. J-Aggregates: From Serendipitous Discovery to Supramolecular Engineering of Functional Dye Materials. *Angew. Chem., Int. Ed.* **2011**, *50* (15), 3376−3410.
(40) Pensack, R. D.; Ashmore, R. J.; Paoletta, A. L.; Scholes, G. D. The Nature of Excimer Formation in Crystalline Pyrene Nanoparticles. *J. Phys. Chem. C* **2018**, *122* (36), 21004−21017.
(41) Rösch, U.; Yao, S.; Wortmann, R.; Würthner, F. Fluorescent H-Aggregates of Merocyanine Dyes. *Angew. Chem., Int. Ed.* **2006**, *45* (42), 7026−7030.
(42) Ryu, N.; Okazaki, Y.; Pouget, E.; Takafuji, M.; Nagaoka, S.; Ihara, H.; Oda, R. Fluorescence Emission Originated from H-Aggregated Cyanine Dye with Chiral Gemini Surfactant Assemblies Having Narrow Absorption Band and Remarkably Large Stokes Shift. *Chem. Commun.* **2017**, *53* (63), 8870−8873.
(43) Huang, Z.; Ji, D.; Wang, S.; Xia, A.; Koberling, F.; Patting, M.; Erdmann, R. Spectral Identification of Specific Photophysics of Cy5 by Means of Ensemble and Single Molecule Measurements. *J. Phys. Chem. A* **2006**, *110* (1), 45−50.
(44) Singh, M. K. Time-Resolved Single Molecule Fluorescence Spectroscopy of Cy5-dCTP: Influence of the Immobilization Strategy. *Phys. Chem. Chem. Phys.* **2009**, *11* (33), 7225−7230.
(45) Turro, N. J.; Scaiano, J. C.; Ramamurthy, V. *Modern Molecular Photochemistry of Organic Molecules*; University Science Books: Sausalito, CA, 2010.
(46) Hestand, N. J.; Spano, F. C. Molecular Aggregate Photophysics beyond the Kasha Model: Novel Design Principles for Organic Materials. *Acc. Chem. Res.* **2017**, *50* (2), 341−350.
(47) Dicke, R. H. Coherence in Spontaneous Radiation Process. *Phys. Rev.* **1954**, *93* (1), 99−110.
(48) Spano, F. C.; Kuklinski, J. R.; Mukamel, S. Cooperative Radiative Dynamics in Molecular Aggregates. *J. Chem. Phys.* **1991**, *94* (11), 7534−7544.
(49) Strickler, S. J.; Berg, R. A. Relationship between Absorption Intensity and Fluorescence Lifetime of Molecules. *J. Chem. Phys.* **1962**, *37* (4), 814−822.
(50) Widengren, J.; Schwille, P. Characterization of Photoinduced Isomerization and Back-Isomerization of the Cyanine Dye Cy5 by Fluorescence Correlation Spectroscopy. *J. Phys. Chem. A* **2000**, *104* (27), 6416−6428.
(51) Sundström, V.; Gillbro, T. Excited State Dynamics and Photophysics of Aggregated Dye Chromophores in Solution. *J. Chem. Phys.* **1985**, *83* (6), 2733−2743.
(52) Dean, J. C.; Oblinsky, D. G.; Rafiq, S.; Scholes, G. D. Methylene Blue Exciton States Steer Nonradiative Relaxation: Ultrafast Spectroscopy of Methylene Blue Dimer. *J. Phys. Chem. B* **2016**, *120* (3), 440−454.
(53) Kreller, D. I.; Kamat, P. V. Photochemistry of Sensitizing Dyes. Spectroscopic and Redox Properties of Cresyl Violet. *J. Phys. Chem.* **1991**, *95* (11), 4406−4410.
(54) Martini, I.; Hartland, G. V.; Kamat, P. V. Ultrafast Photophysical Investigation of Cresyl Violet Aggregates Adsorbed onto Nanometer-Sized Particles of SnO2 and SiO2. *J. Phys. Chem. B* **1997**, *101* (24), 4826−4830.
(55) Das, S.; Kamat, P. V. Can H-Aggregates Serve as Light-Harvesting Antennae? Triplet−Triplet Energy Transfer between Excited Aggregates and Monomer Thionine in Aersol-OT Solutions. *J. Phys. Chem. B* **1999**, *103* (1), 209−215.
(56) Nasr, C.; Hotchandani, S. Excited-State Behavior of Nile Blue H-Aggregates Bound to SiO2 and SnO2 Colloids. *Chem. Mater.* **2000**, *12* (6), 1529−1535.
(57) Kelbauskas, L.; Bagdonas, S.; Dietel, W.; Rotomskis, R. Excitation Relaxation and Structure of TPPS4 J-Aggregates. *J. Lumin.* **2003**, *101* (4), 253−262.
(58) Collini, E.; Ferrante, C.; Bozio, R. Influence of Excitonic Interactions on the Transient Absorption and Two-Photon Absorption Spectra of Porphyrin J-Aggregates in the NIR Region. *J. Phys. Chem. C* **2007**, *111* (50), 18636−18645.
(59) Verma, S.; Ghosh, A.; Das, A.; Ghosh, H. N. Ultrafast Exciton Dynamics of J- and H-Aggregates of the Porphyrin-Catechol in Aqueous Solution. *J. Phys. Chem. B* **2010**, *114* (25), 8327−8334.
(60) Kakade, S.; Ghosh, R.; Palit, D. K. Excited State Dynamics of Zinc-Phthalocyanine Nanoaggregates in Strong Hydrogen Bonding Solvents. *J. Phys. Chem. C* **2012**, *116* (28), 15155−15166.
(61) Caplins, B. W.; Mullenbach, T. K.; Holmes, R. J.; Blank, D. A. Intermolecular Interactions Determine Exciton Lifetimes in Neat Films and Solid State Solutions of Metal-Free Phthalocyanine. *J. Phys. Chem. C* **2015**, *119* (49), 27340−27347.
(62) Sanchez-Galvez, A.; Hunt, P.; Robb, M. A.; Olivucci, M.; Vreven, T.; Schlegel, H. B. Ultrafast Radiationless Deactivation of Organic Dyes: Evidence for a Two-State Two-Mode Pathway in Polymethine Cyanines. *J. Am. Chem. Soc.* **2000**, *122* (12), 2911−2924.

DOI: 10.1021/acs.jpclett.9b00404
J. Phys. Chem. Lett. 2019, 10, 2386−2392